Dynamic compression of soft layered materials yields tunable and spatiotemporally evolving surface patterns

Brianna MacNider, Xudong Liang, Samantha Hoang, Maroun Abi Ghanem, Shengqiang Cai, and Nicholas Boechler

Phys. Rev. E **107**, 035002 — Published 17 March 2023

DOI: 10.1103/PhysRevE.107.035002

Dynamic Compression of Soft Layered Materials Yields Tunable and Spatiotemporally Evolving Surface Patterns

Brianna MacNider[1], Xudong Liang[1], Samantha Hoang[2], Maroun Abi Ghanem[3], Shengqiang Cai[1], and Nicholas Boechler[1]

1) Department of Mechanical and Aerospace Engineering, University of California San Diego, 9500 Gilman Drive, La Jolla, CA 92093

2) Department of Mechanical Engineering, University of Washington, 1959 NE Pacific St, Seattle, WA 98195 and

3) Université Claude Bernard Lyon 1, CNRS, Institut Lumière Matière, F-69622 Villeurbanne, France

(Dated: February 2, 2023)

Soft layered systems buckling to form surface patterns has been widely studied under quasi-static loading. Here, we study the dynamic formation of wrinkles in a stiff-film-on-viscoelastic-substrate system as a function of impact velocity. We observe a novel spatiotemporally varying range of wavelengths, which display impactor velocity dependence and exceed the range exhibited under quasi-static loading. Simulations suggest the importance of both inertial and viscoelastic effects. Film damage is also examined, and we find that it can tailor dynamic buckling behavior. We expect our work to have applications to soft elasto-electronic and optic systems and open new routes for nanofabrication.

Mechanical surface instabilities are commonly observed in soft, solid systems containing interfaces [1] and can lead to the formation of periodic surface morphologies, including wrinkles [2–5], ridges [6, 7], and folds [8]. Such surface instabilities are both widely observed in nature [9–11] and have been proposed for use in a variety of applications, ranging from material property metrology [12, 13] to flexible electronics [14–16] and nanofabrication [17]. A canonical setting for exploring such mechanics has been stiff films layered on a softer substrate [18] (including studies where the substrate is liquid [19, 20]). For the stiff-film-on-soft-substrate system, the surface patterns start as a single wavelength sinusoid, then follow a known path within increasing strain, dictated by the material properties, layer thickness, and boundary conditions, which results in period doubling, quadrupling, or transitions into periodic arrays of folds [8] (such modes have not been shown for films on liquids).

Studies exploring the dynamic response of stiff-film-on-soft-substrate systems have introduced further complexity and shown that dynamic loading can lead to progressive formation, and evolving wavelengths, of the sinusoidal surface wrinkling patterns [21–23]. Analogies to this complexity introduced by dynamic loading can also be seen by contrasting quasi-static and dynamic buckling of thin bars [24, 25], filaments [26], smectic bubbles [27], and films [21, 28] in fluids, albeit their taxonomy is less diverse than that of stiff films on soft substrates.

In this work, we demonstrate how high-amplitude dynamic loading of stiff-film-on-soft-substrate systems yields hitherto unreported surface patterns. As in Ref. [22], our system consists of a polydimethylsiloxane (PDMS) block bonded to a stiffer film (herein we use a Kapton film, whereas the prior study used a softer, PDMS film). The system is impacted with a striker plate, resulting in the propagation of a bulk wave and initiation of wrinkling patterns on the surface (shown in Fig. 1). The response was captured via high speed video, analyzed via digital image processing, and then modeled using finite element method (FEM) simulations. In both experiment and simulation, we observe the dynamic formation of surface patterns containing numerous, non-integer-multiple wavelengths that evolve across both space and time, are tunable with striker velocity, and are shorter than those exhibited under quasi-static loading. We also study how the presence of even small amounts of deviation from a flat film profile, such as may be caused by prior testing or intentionally designed into the system [29–31] has a drastic effect on the subsequent dynamic surface morphology evolution.

The PDMS blocks used are of length $L = 50.4$ mm, square cross section of side length $w = 37$ mm, and are bonded on one side to a stiffer Kapton tape film with a thickness of $t = 102$ μm. Six nominally identical samples [32] were fabricated to perform tests at varying impact velocities without contaminating the results with potential damage induced by prior impacts. To confirm comparability between samples, quasi-static compression tests were performed on each sample. Quasi-static testing past the point of period doubling was only conducted on "sample 1" (the sample impacted at 1.9 m/s, see Fig. 1A and C). Each sample was subsequently tested by impacting them in their "pristine" state (not previously exposed to dynamic loading) at speeds varying from 1.9 to 8.9 m/s. The striker compressed the samples about $\delta L = 8.6 \pm 0.1$ mm before being halted by stoppers (Fig. 1B). The impact sent a large amplitude, low frequency compression wave through each sample, which caused the film to form wrinkles. After imaging the sample at 30 kfps, an edge detection algorithm was used to track the surface profile for all images. The low frequency portion of the displacement was subtracted to isolate the wrinkles for further analysis, and a spatial fast Fourier transform (FFT) was then performed at each time step.

The described image analysis procedure was used to obtain the wrinkling amplitude A as a function of quasi-static strain ϵ. For convenience, we take $\epsilon > 0$ as compression. The measured response in Fig. 1C (markers)

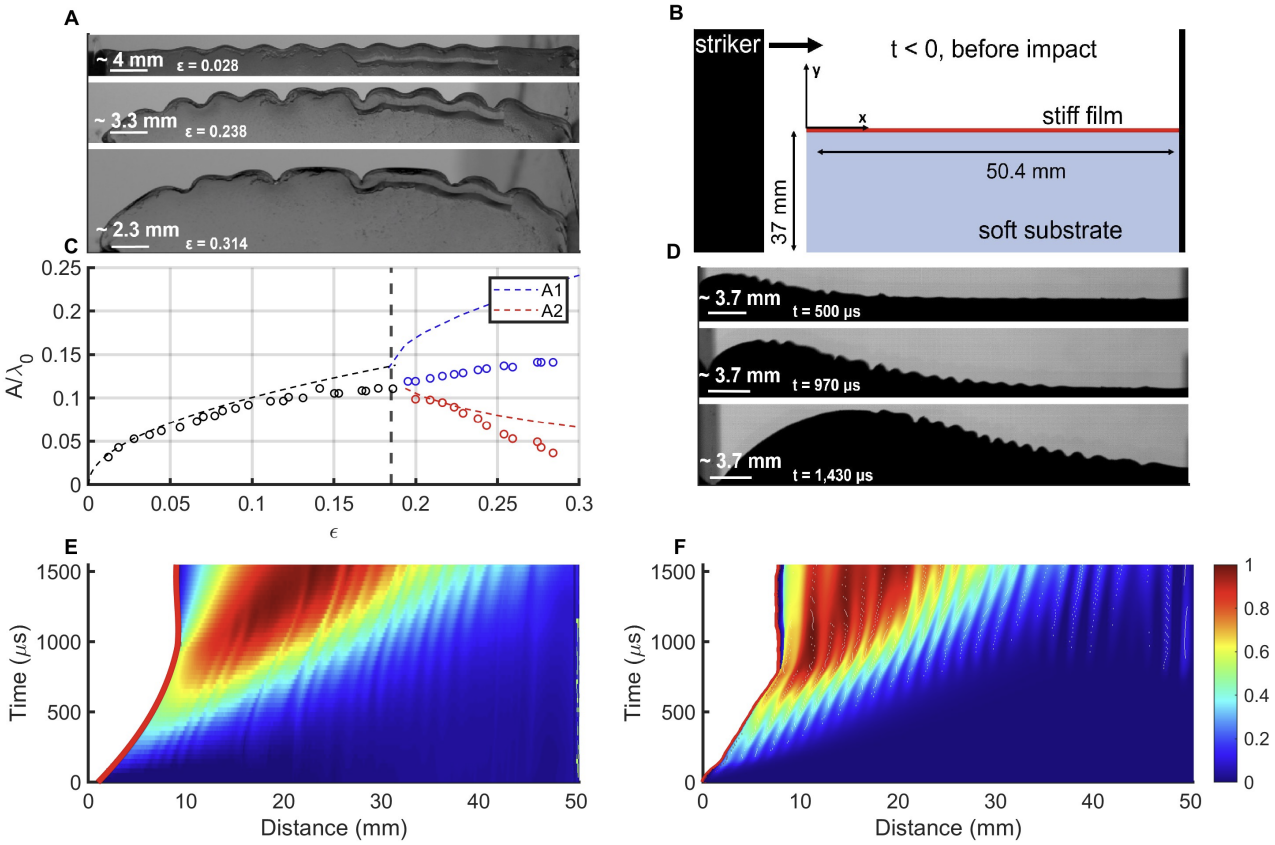

FIG. 1. A) Pre-impact-test quasi-static compression of "sample 1" yields period doubling behavior. B) The dynamic test setup. C) Measured (markers) and predicted (dashed lines) quasi-static wrinkle amplitude vs. strain, corresponding to the test of panel A. After the critical strain (vertical thick dashed line), the period doubled mode (blue, top branch) grows and the original mode (red, bottom branch) fades. D) Snapshots from a test at 7.1 m/s impactor velocity on a "pristine" sample, displaying multiple wavelength surface patterns. E) A normalized spatiotemporal diagram of the experiment shown in D, with color representing the y-direction surface displacement, U_y. The line visible at the right edge is an artifact the camera frame edge and should be disregarded. F) A normalized spatiotemporal diagram of the simulation (7.6 m/s impact velocity, same color scheme as in E).

mirrors prior studies [8, 33], where at a critical strain ϵ_0 the sample buckles to a mode of wavelength λ_0. For sample 1, $\lambda_{0,1} = 4.1$ mm (where the second subscript denotes the sample number), whereas the initial buckling wavelength averaged across all samples was $\lambda_{0,avg} = 3.8$ mm (standard deviation of 0.24 mm). Sample 1 exhibits period doubling to a wavelength of $\lambda_{1,1}$ at strain $\epsilon_1 = 0.185$, and then eventual period quadrupling. The dashed lines in Fig. 1C denote predictions from analytical model of Ref. [33], using the measured $\lambda_{0,1}$. We attribute the post-period-doubling deviations between the measurements and the model to reduced compression at the sample surface due to the sample curling around the edge of the compression plates.

Representative images from the impact experiments are shown in Fig. 1D, which display shorter wavelengths than the quasi-static case (Fig. 1A), and the wrinkling wavelength appears to vary across time and the length of the sample. Using the same image analysis procedure for the quasi-static case, this variation is also observable in a spatiotemporal plot of the measured out-of-plane surface displacement (Fig. 1E). These qualitative observations hold across all experiments performed, although the wavelengths present vary.

The impact tests were modeled via FEM simulations (Abaqus/CAE) [32]. A moving boundary matching impactor profile of the first (and slowest) dynamic experiment was applied, which was subsequently scaled up for higher velocity impact cases. In Fig. 1F, we show the simulated spatiotemporal evolution of the out-of-plane surface displacement for a similar impact velocity to that used in the experiment of Fig. 1D and E.

In Fig. 2, we show spatial FFT spectra of the quasi-static compression test (corresponding to the data in Fig. 1A,C) and simulated and experimental dynamic compression tests (2.5 m/s and 1.9 m/s impactor velocities, respectively). In Fig. 2A, the emergence of period doubled and quadrupled modes with increasing applied quasi-static strain can be seen. In Fig. 2B and C, corresponding to the impact experiment and sim-

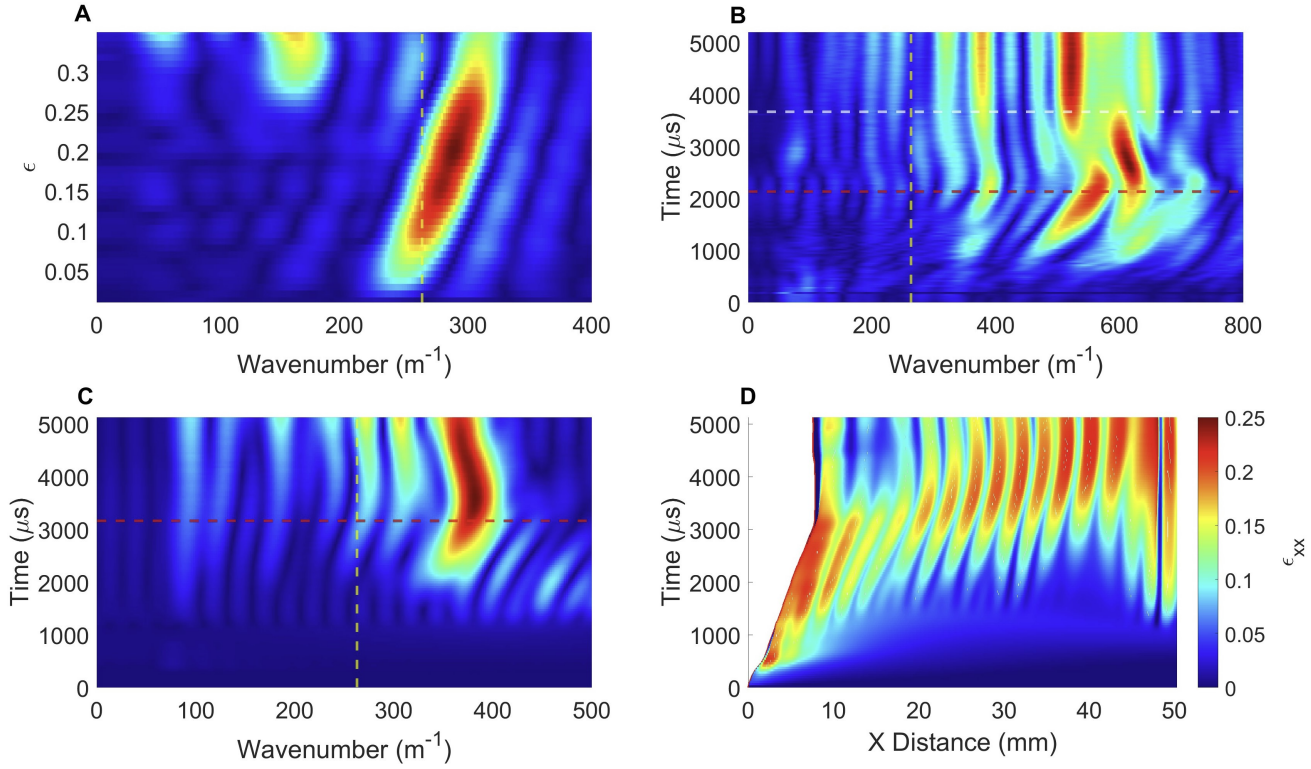

FIG. 2. A) FFT of the sample 1 quasi-static compression test. FFT of a dynamic test (B) and FEM simulation (C), with impact speeds of 2.5 m/s and 1.9 m/s, respectively. Wavenumber ~ 263 m^{-1} corresponds to $\lambda_{0,avg}$, and is shown as the dashed vertical yellow lines in A, B, and C. The horizontal red dashed lines in B (lower horizontal dashed line) and C (sole horizontal dashed line) represent the time at which the striker hits the stop blocks and comes to a stop, while the white (upper) horizontal dashed line in B represents the time of arrival at the right edge of the peak of the bulk compression wave. This same bulk wave arrival time in C and D is the upper limit of the times shown. D) Spatiotemporal evolution of strain obtained from the FEM simulation in C, averaged over a depth of $\lambda_{0,1}$ (compression shown as positive).

ulation, respectively, a complex spatiotemporal evolution involving multiple wavelengths is observed, marking a stark, qualitative difference to the quasi-static response. The wavenumbers (here, defined as $1/\lambda$) emerging from the dynamic tests uniformly exceed the quasi-static wavenumbers. The simulated local strain ϵ (normal strain in the x-direction, averaged over a depth of $\lambda_{0,avg}$ in the y-direction) is shown in Fig. 2D to reach values higher than ϵ_1. Thus, while the average sample strain is less than ϵ_1 in the cases of Fig. 2B and C, localized period doubling might be expected. However, none of the observed modes were found to be obvious factor of two multiples of the others. The sole exception to this is sample 1 [32], which displayed one dominant buckling wavelength, out of many, that approached the period doubled mode wavelength. We suggest this is because sample 1 was the sole case to be quasi-statically tested past the period doubling point prior to dynamic testing (this observation is later explored more fully).

The impact tests of Fig.2 showed an upward wavenumber shift from the quasi-static response. The range of wavelengths of the most prominent peaks emerging from the impact experiments are consistently $2-4$ times smaller than $\lambda_{0,avg}$ (~ 1 to 2 mm), even after the passage of the bulk compression wave when relaxation dominates. Quantifying the measured spectra from experimental and simulated impact tests, we take the spectral centroid of each spectrum, for each time step, and examine the averages and maximums. We note that the maximum values consist of phenomena mainly driven by the compression regime, while the average values contain data from both the compression and relaxation regimes. The limits of the considered wavenumber range for the spectral centroid analysis are set to 50% of the maximum amplitude in each case. Figure 3A shows a positive dependence of the maximum (compression dominated regime) wavenumber spectral centroid on velocity. We note a change in the observed striker velocity dependence in the experimental data at 5.6 m/s, which corresponds to the test at which the striker recoil first results in a complete detachment between the striker and sample. This detachment introduces a competing tension which reduces the strength of the compression regime. All simulations were run without this recoil in order to study the expected trend had recoil not been present, and a clear speed dependent increase in wavenumber is observed (Fig. 3B). We also note a drop in the wrinkle amplitude as impact velocity

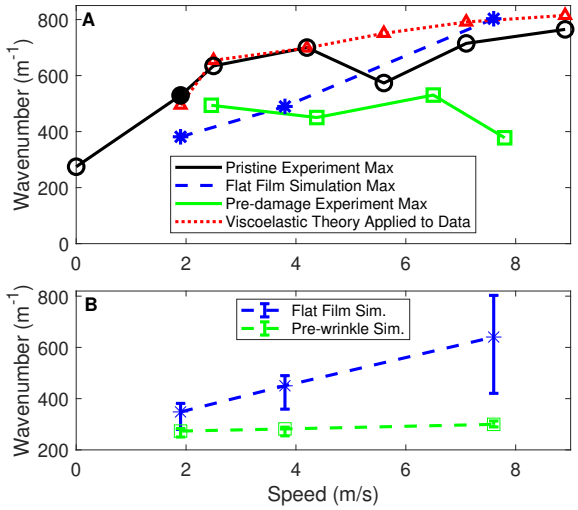

FIG. 3. A) The maximum spectral centroid (in time) of the dynamically tested samples. Shown are results from pristine sample experiments (black, circles), pre-damaged sample experiments (green, squares), flat film simulations (blue, stars), and substitution of measured ω into Eq. 1 (red, triangles). B) Wavenumber spectral centroids for flat film simulations (blue, stars) and pre-wrinkle film simulations (green, squares), with the average and the range between minimum and maximum values indicated by the error bars.

is increased, highlighted in Figure S9 in the SM [32].

We suggest that the increase in observed wavenumber with increasing impact speed (and with respect to quasi-static loading) can, in part, be accounted for by the viscoelasticity of the substrate. We model our substrate as a standard linear solid (SLS) material, where the magnitude of the dynamic elastic modulus can be described as [34]:

$$E^* = \mid E_1 + E_0\left(\frac{\omega^2{\tau_r}^2}{1+\omega^2{\tau_r}^2}\right) + iE_0\left(\frac{\omega\tau_r}{1+\omega^2{\tau_r}^2}\right) \mid, \quad (1)$$

$E_1 = 10$ MPa , $E_0 = 130$ KPa $\tau_r = 90$ μs, and the characteristic excitation frequency ω is estimated by taking the temporal FFT of the striker position until rest (ignoring recoil), and identifying the frequency at half amplitude maximum. This approximation predicts a critical buckling wavenumber of 500 to 760 m^{-1} (across all tests, shown in Fig. 3A), in good agreement with the measurements. Wavelength shift due to impact in systems containing viscous substrates has been noted in several other works. The authors of Ref. [24] examine an elastic filament in a viscous fluid compressed at various strain rates, and similarly find a decrease in buckling wavelength with increased strain rate. In Ref.[23], the effect of strain rate upon the compression of soft layered composites is studied, and viscoelastic stiffening is predicted to adjust the critical buckling wavelength with increased strain rate. In Ref. [21], a dynamic wavelength smaller than the quasi-static wavelength is observed, though wavelength dependence on impactor velocity is not present due to the domination of inertial over viscous effects.

Despite the described agreement, we suggest that viscoelasticity cannot be the sole contributing effect to the observed velocity dependence. Comparative simulations were conducted in which the viscoelastic behavior was removed from the substrate material properties (leaving a hyperelastic-only substrate model). A similar, though greatly reduced, downshift in wavelength was observed with increasing impact speeds [32]. Similarly, using the simulated response of the hyperelastic-only sample, we compare the maximum spectral centroid at similar strain levels between dynamic and quasi-static cases (Fig. 4A). At comparable strain levels, hyperelastic-only simulations display a larger wavenumber in the dynamic case than in the quasi-static case, asserting that substrate nonlinearity alone cannot account for the observed wavenumber shift (even in the absence of viscoelastic effects). This suggests a third contributing factor, which we posit may result from inertial effects. Using the simulated material properties and the characteristic excitation frequency, where $f = \omega/(2\pi)$, to estimate the relative magnitude of viscous, inertial, and elastic effects (Fig 4B), we find that as impact velocity is increased, the importance of inertial effects increases relative to viscous and elastic effects (see [32] for more information).

In contrast to the wavelength velocity dependence, broadband wavenumber content is not present in the aforementioned literature. Although wavelength is observed to evolve with time [21, 23, 24], it does not signficantly vary spatially. A spatial wavelet analysis was performed on the experiments herein that confirms the presence of spatial wavenumber variation at a given time [32]. We note that the nature of our experimental setup, in particular the presence of relaxation processes and bulk compression wave reflection, somewhat complicates the examination of wavelength variation. References [27] and [26] noted wavelength variation as a function of global system contraction and expansion by observing the unchanging number of peaks across a given region. Separating out these regimes, therefore, is important in the effort to identify the presence and source of any spatial wavelength variation. We therefore take care to mark in all FFT analyses several times important to the separation of the pure compression and pure relaxation regimes, including the time at which the striker comes to a stop (and, in some cases, rebounds, inducing an earlier onset of the relaxation regime) and the time at which the peak of the bulk compression wave reaches the sample edge (after which reflection, and a relaxation dominated regime, ensues). We consider phenomena occurring in the times before striker stop as being mainly compression driven, the times between striker stop and bulk wave rebound as being a mixture of compression and relaxation, and the times after bulk wave rebound as being relaxation dominated. Although pronounced wavelength variation is seen after the rebound of the bulk compression wave sends the entire sample into a relaxation regime, and we do note

the expansion of wrinkles post passage of the bulk wave, significant variation in wavelength is present during early times in the region ahead of the bulk wave, when the initial striking of the sample drives a compression dominated regime. In addition, we observe multiple distinct wavelengths which are not the result of a smooth transition between compressed and extended wrinkles of a single base wavelength. It is therefore unlikely that global and local length changes are the sole underlying cause of the spatial variation we see. Several other possible causes are considered. The strain rate herein varies from 38 s^{-1} to 180 s^{-1}. This is much greater than the strain rates of Refs. [23, 24], and, although the maximum impact velocity in Ref. [21] is comparable to our lowest impact velocity, it is noted that inertia, rather than viscosity, dominates their system's response. We suggest the high impact velocity induces a spatial variation in viscoelastic stiffening, altering the effective localized elastic modulus, creating many localized "λ_0" values. This could also enhance the nonlinear response of the system, by effectively dropping ϵ_0 [23]. This could also induce nonlinear interactions between spatially neighboring modes [35]. Such nonlinearity is absent, or much weaker, in systems with a fluid substrate (as in Ref. [21]).

Further evidence of viscoelasticity serving as the driving factor for spatial wavenumber heterogeneity can be seen by comparing spatiotemporal variation of the wrinkling patterns, instantaneous dynamic modulus, and inertial forces found from simulations with combinations of elastic, hyperelastic, and viscoelastic properties [32]. Specifically, only in the cases with viscoelasticity are low amplitude longitudinal waves racing ahead of the large-deformation bulk wave seen to alter, and induce a more complex spatial variation of, the instantaneous properties of the substrate before wrinkle formation. This is seen to result in a spatial wavelength heterogeneity in the case of the viscoelastic simulations during initial passage of the large-deformation bulk wave, which is not present in the elastic and hyperelastic cases [32].

Both the wavelength decrease and spatial variation observed in this work were not observed in the prior, related study of Ref. [22]. In this previous case, a single main wavelength was observed evolving across time, but with minimal spatial variation. As the substrates are nominally identical between the two studies, we look elsewhere for the cause of the discrepancy. It was noted in Ref. [22] that the sample studied therein was tested quasi-statically and dynamically multiple times, while the samples in this paper were tested to low strain (excluding sample 1), quasi-statically, a single time, and then dynamically only once to reach the prior results. Visual inspection of both current and previous samples after testing reveals small but observable indentations on the surface of the film [32], suggesting damage due to previous testing could be the cause of the observed differences. In order to explore the effect of pre-damage on the impact response, further experiments and simulations were performed. Simulations were run with an initial 'pre-

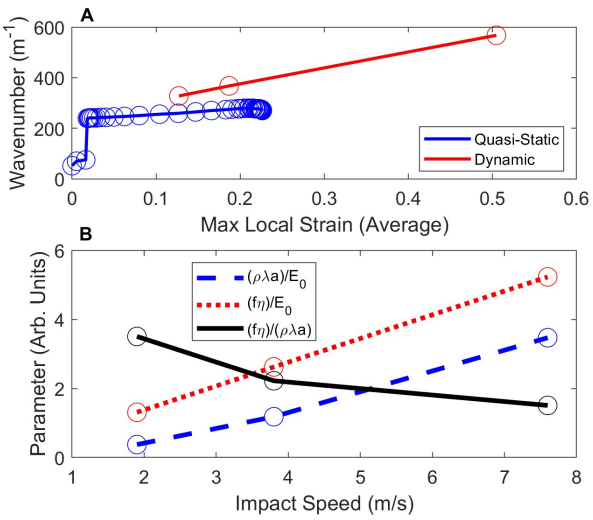

FIG. 4. A) Wavenumber maximum spectral centroid as a function of maximum local strain averaged over a depth of $\lambda_0, 1$ for purely hyperelastic substrate simulations, showing that even without viscoelasticity the combination of nonlinearity and inertial effects present in dynamic cases (red, upper line) can induce wavenumbers significantly exceeding quasi-static compression (blue, lower line). B) Dimensionless parameters estimating inertial ($\rho\lambda a$), viscous ($f\eta$), elastic (E_0)), where a is the maximum acceleration of the striker, λ the wavenumber maximum spectral centroid, and ρ the material density, showing that as impact speed is increased both inertial and viscous forces increase with respect to elastic forces, with inertial forces increasing at a faster rate than viscous ones.

wrinkle' profile applied to the film. This pre-wrinkle profile was given a wavelength matching the expected quasi-static critical buckling wavelength, with amplitude set to a fraction of the thickness of the film. As observed in Ref. [22], a single prominent wavelength occurred near the quasi-static buckling wavelength, matching the pre-wrinkled pattern. Figure 3B shows the spectral centroid time average and range for both pre-wrinkled and flat film simulations, wherein the pre-wrinkled case shows a drastically reduced velocity dependence. Time averages were taken across the entirety of simulation run time, encompassing the full temporal evolution of the wavenumber landscape. As flat-film and pre-wrinkle simulations were run under the exact same conditions for each impact speed, with the only difference being the presence of film pre-wrinkling, time averages capture the same range of data between the flat-film and pre-wrinkle cases, and the stark effect of the introduction of pre-wrinkling is clear. The examination of both the average and range of the spectral centroid highlights that this reduced velocity dependence holds across both compression (represented by the maximum centroid value) and relaxation (represented by the minimum centroid value) regimes. Retesting the previously-only-once-impacted samples, the maximum spectral centroid is shown in comparison to that

of the pristine samples in Fig. 3A, which reveals a lowered value of the maximum spectral centroid, as well as reduced velocity dependence. We note a key difference between the "retested" samples herein, and those of Ref. [22] is that the predamage was found to be aperiodic and periodic, respectively, thus giving different wavenumber distributions but an otherwise similar qualitative response. In addition, we remind the reader that sample 1 was the only first-tested sample in this work to display significant long wavelength buckling prior to striker rebound. Given that sample 1 was the only sample tested past the quasi-static period doubling point, it may contain weak pre-damage consistent with the first or second quasi-static buckling mode, and its wavelength content would therefore be expected to differ somewhat from the entirely "pristine" samples.

Through dynamic testing of stiff-film-on-soft substrate systems, we observe the emergence of hitherto unobserved spatiotemporally varying surface patterns. The system's velocity dependence, which we tie to viscous and inertial effects, may hold promise in the potential dynamic tuning of surface patterns in a system that classically can only be adjusted through change of its material properties. The complexity of the underlying causes may provide motivation for improved nonlinear dynamical and viscous models capable of predicting the dynamic surface morphology evolution, which may further enable the informed design of new surface patterns as may be applicable to flexible electronics (e.g. nonlinear signal processing) and nanofabrication.

ACKNOWLEDGMENTS

We thank John Hutchinson for insightful discussions. We acknowledge Guangcan Lu for early experiments exploring the impact response of PDMS blocks with Kapton tape surface films. This work was supported by the US National Science Foundation (Grant No. CMMI-1536406) and the US Army Research Office (Grant No. W911NF-20-2-0182).

[1] B. Li, Y.-P. Cao, X.-Q. Feng, and H. Gao, "Mechanics of morphological instabilities and surface wrinkling in soft materials: a review," *Soft Matter*, vol. 8, pp. 5728–5745, 2012.

[2] Z. Huang, W. Hong, and Z. Suo, "Nonlinear analyses of wrinkles in a film bonded to a compliant substrate," *Journal of the Mechanics and Physics of Solids*, vol. 53, pp. 2101–2118, Sept. 2005.

[3] J. W. Hutchinson, "The role of nonlinear substrate elasticity in the wrinkling of thin films," *Philosophical Transactions of the Royal Society A: Mathematical, Physical and Engineering Sciences*, vol. 371, p. 20120422, June 2013.

[4] S. Yang, K. Khare, and P.-C. Lin, "Harnessing Surface Wrinkle Patterns in Soft Matter," *Adv. Funct. Mater.*, vol. 20, pp. 2550–2564, Aug. 2010.

[5] N. Bowden, S. Brittain, A. G. Evans, J. W. Hutchinson, and G. M. Whitesides, "Spontaneous formation of ordered structures in thin films of metals supported on an elastomeric polymer," *Nature*, vol. 393, pp. 146–149, May 1998.

[6] Y. Cao and J. W. Hutchinson, "Wrinkling Phenomena in Neo-Hookean Film/Substrate Bilayers," *Journal of Applied Mechanics*, vol. 79, p. 031019, May 2012.

[7] J. Zang, X. Zhao, Y. Cao, and J. W. Hutchinson, "Localized ridge wrinkling of stiff films on compliant substrates," *Journal of the Mechanics and Physics of Solids*, vol. 60, pp. 1265–1279, July 2012.

[8] F. Brau, P. Damman, H. Diamant, and T. A. Witten, "Wrinkle to fold transition: influence of the substrate response," *Soft Matter*, vol. 9, no. 34, p. 8177, 2013.

[9] J. Yin, Z. Cao, C. Li, I. Sheinman, and X. Chen, "Stress-driven buckling patterns in spheroidal core/shell structures," *Proceedings of the National Academy of Sciences*, vol. 105, pp. 19132–19135, Dec. 2008.

[10] A. Boudaoud, "An introduction to the mechanics of morphogenesis for plant biologists," *Trends in Plant Science*, vol. 15, pp. 353–360, June 2010.

[11] L. Wang, C. E. Castro, and M. C. Boyce, "Growth strain-induced wrinkled membrane morphology of white blood cells," *Soft Matter*, vol. 7, no. 24, p. 11319, 2011.

[12] J. Y. Chung, A. J. Nolte, and C. M. Stafford, "Surface Wrinkling: A Versatile Platform for Measuring Thin-Film Properties," *Advanced Materials*, vol. 23, pp. 349–368, Jan. 2011.

[13] A. Schweikart and A. Fery, "Controlled wrinkling as a novel method for the fabrication of patterned surfaces," *Microchimica Acta*, vol. 165, pp. 249–263, June 2009.

[14] S. P. Lacour, S. Wagner, Z. Huang, and Z. Suo, "Stretchable gold conductors on elastomeric substrates," *Applied Physics Letters*, vol. 82, pp. 2404–2406, Apr. 2003.

[15] D. Kim and J. A. Rogers, "Stretchable Electronics: Materials Strategies and Devices," *Advanced Materials*, vol. 20, pp. 4887–4892, Dec. 2008.

[16] D.-Y. Khang, J. A. Rogers, and H. H. Lee, "Mechanical Buckling: Mechanics, Metrology, and Stretchable Electronics," *Adv. Funct. Mater.*, vol. 19, pp. 1526–1536, May 2009.

[17] S. Singamaneni, M. E. McConney, and V. V. Tsukruk, "Spontaneous Self-Folding in Confined Ultrathin Polymer Gels," *Adv. Mater.*, vol. 22, pp. 1263–1268, Mar. 2010.

[18] J. Genzer and J. Groenewold, "Soft matter with hard skin: From skin wrinkles to templating and material characterization," *Soft Matter*, vol. 2, no. 4, p. 310, 2006.

[19] R. Huang and Z. Suo, "Wrinkling of a compressed elastic film on a viscous layer," *Journal of Applied Physics*, vol. 91, pp. 1135–1142, Feb. 2002.

[20] O. Kodio, I. M. Griffiths, and D. Vella, "Lubricated wrinkles: Imposed constraints affect the dynamics of wrinkle coarsening," *Phys. Rev. Fluids*, vol. 2, p. 014202, Jan. 2017.

[21] F. Box, D. O'Kiely, O. Kodio, M. Inizan, A. A. Castrejón-Pita, and D. Vella, "Dynamics of wrinkling in ultrathin

elastic sheets," *Proceedings of the National Academy of Sciences*, vol. 116, pp. 20875–20880, Oct. 2019.

[22] M. Abi Ghanem, X. Liang, B. Lydon, L. Potocsnak, T. Wehr, M. Ghanem, S. Hoang, S. Cai, and N. Boechler, "Wrinkles riding waves in soft layered materials," *Advanced Materials Interfaces*, vol. 6, no. 1, p. 1801609, 2019.

[23] V. Slesarenko and S. Rudykh, "Harnessing viscoelasticity and instabilities for tuning wavy patterns in soft layered composites," *Soft Matter*, vol. 12, no. 16, pp. 3677–3682, 2016.

[24] J. Chopin, M. Dasgupta, and A. Kudrolli, "Dynamic Wrinkling and Strengthening of an Elastic Filament in a Viscous Fluid," *Phys. Rev. Lett.*, vol. 119, p. 088001, Aug. 2017.

[25] H. E. Lindberg, "Impact Buckling of a Thin Bar," *Journal of Applied Mechanics*, vol. 32, pp. 315–322, 06 1965.

[26] Salili, S. M. and Ostapenko, T. and Kress, O. and Bailey, C. and Weissflog, W. and Harth, K. and Eremin, A. and Stannarius, R. and Jákli, A.,"Rupture and recoil of bent-core liquid crystal filaments," *Soft Matter*, vol. 12, pp. 4725–4730, 2016.

[27] Harth, Kirsten and Trittel, Torsten and May, Kathrin and Stannarius, Ralf, "Dynamic wrinkling of freely floating smectic films," *Soft Matter*, vol. 15, pp. 6769–6778, 2019.

[28] L. Deike, J.-C. Bacri, and E. Falcon, "Nonlinear waves on the surface of a fluid covered by an elastic sheet," *J. Fluid Mech.*, vol. 733, pp. 394–413, Oct. 2013. arXiv: 1309.6990.

[29] C.-M. Chen, J. C. Reed, and S. Yang, "Guided wrinkling in swollen, pre-patterned photoresist thin films with a crosslinking gradient," *Soft Matter*, vol. 9, no. 46, p. 11007, 2013.

[30] E. Flores-Johnson, T. J. Rupert, K. J. Hemker, D. S. Gianola, and Y. Gan, "Modelling wrinkling interactions produced by patterned defects in metal thin films," *Extreme Mechanics Letters*, vol. 4, pp. 175–185, Sept. 2015.

[31] J.-H. Lee, H. W. Ro, R. Huang, P. Lemaillet, T. A. Germer, C. L. Soles, and C. M. Stafford, "Anisotropic, Hierarchical Surface Patterns via Surface Wrinkling of Nanopatterned Polymer Films," *Nano Letters*, vol. 12, pp. 5995–5999, Nov. 2012.

[32] "See Supplemental Material at [URL will be inserted by publisher] for further information on sample fabrication, simulation details, detailed results of all experiments and simulations, and videos of the experiments.," 2023.

[33] F. Brau, H. Vandeparre, A. Sabbah, C. Poulard, A. Boudaoud, and P. Damman, "Multiple-length-scale elastic instability mimics parametric resonance of nonlinear oscillators," *Nature Physics*, vol. 7, pp. 56–60, Jan. 2011.

[34] R. Lakes, *Viscoelastic Materials*. Cambridge University Press, 2009.

[35] N. Boechler, G. Theocharis, and C. Daraio, "Bifurcation-based acoustic switching and rectification," *Nature Mater*, vol. 10, pp. 665–668, Sept. 2011.